Transient electrohydrodynamics of a liquid drop

Asghar Esmaeeli* and Payam Sharifi
Department of Mechanical Engineering and Energy Processes, Southern Illinois University, Carbondale, Illinois 62901, USA
(Received 16 February 2011; revised manuscript received 15 June 2011; published 9 September 2011)

The transient behavior of a leaky dielectric liquid drop under a uniform electric field of small strength is investigated. It is shown that for small distortion from a spherical shape, the drop deforms to an ellipsoid, and the deformation time history is represented by $\mathcal{D} = \mathcal{D}_\infty[1 - \exp(-t/\tau)]$, where $\mathcal{D}_\infty$ is the steady-state deformation and $\tau = (a\mu_o/\gamma)(19\widetilde{\mu} + 16)(2\widetilde{\mu} + 3)/(40\widetilde{\mu} + 40)$ is the characteristic time, a, γ, μ_o and $\widetilde{\mu}$ being the drop radius, the surface tension, the viscosity of ambient fluid, and ratio of the drop viscosity to that of the ambient fluid, respectively. The contributions of the net normal and tangential electrical stresses in the degree of deformation and fluid flow strength are also determined.

DOI: 10.1103/PhysRevE.84.036308 PACS number(s): 47.65.−d, 82.70.−y, 83.50.−v, 47.57.−s

I. INTRODUCTION

When a droplet of a fluid is suspended in another fluid and is subjected to an electric field, the mismatch between the dielectric properties of the fluids results in "net" normal and tangential electrical stresses at the drop surface, which sets the fluids in motion and leads to deformation and possible burst of the drop. The theoretical model that describes the phenomenon fairly well is the so-called "leaky-dielectric theory," pioneered by Taylor [1] and extensively used by Melcher to develop the electrohydrodynamic theory. See, for example, Refs. [2–5]. The essence of the model is to assume that fluids have finite electric conductivities and that the time scale of charge relaxation due to electric conduction from the bulk to the drop surface to be much shorter than the convective time scale. The first assumption allows for the accumulation of free charges at the interface and, therefore, the possibility of net electrical shear forces at the interface. The second assumption leads to a substantial simplification of the mathematical formulation as the electric field equations will be decoupled from the momentum equation and reduce to quasi-steady-state laws [2]. Taylor [1] solved the steady-state electrohydrodynamic equations for the fluid inside and outside a spherical liquid drop in the creeping flow limit using axisymmetric spherical coordinates (Fig. 1) and showed that the relative importance of the ratios of electric conductivities ($R = \sigma_i/\sigma_o$) and permittivities ($S = \epsilon_i/\epsilon_o$) of the fluids is a key parameter in setting the senses of drop deformation and fluid circulation. Specifically, he showed that the electric field establishes a circulatory flow in the drop, consisting of four vortices of equal strengths that are matched by counterpart vortices in the ambient fluid. For $R < S$, the direction of the ambient flow is from the poles to the equator, while for $R > S$ the flow direction is the opposite. He also found a characteristic function

$$\Phi = R^2 + 1 - 2S + \frac{3}{5}(R - S)\frac{3\widetilde{\mu} + 2}{\widetilde{\mu} + 1}, \tag{1}$$

which he used to predict the sense of the drop deformation. For $\Phi < 0$, the drop deforms to an oblate spheroid (i.e., an ellipsoid with its major axis perpendicular to the direction of the electric field), while for $\Phi > 0$ it deforms to a prolate spheroid (i.e., an ellipsoid with its major axis parallel to the direction of the electric field). Here $\Phi = 0$ represents a zero deformation state, which is a possibility for leaky dielectric fluids, where the Coulomb forces and polarization forces can act in the opposite directions. Vizika and Saville [6] used Taylor's solution and found an estimate for the steady-state deformation of the drop:

$$\mathcal{D}_\infty = \frac{9\mathrm{Ca}}{16}\frac{\Phi}{(R + 2)^2}, \tag{2}$$

by balancing the normal stresses at the drop surface posteriorly. In Eq. (2), the deformation is defined as $\mathcal{D} = (z_{\max} - r_{\max})/(z_{\max} + r_{\max})$, where $z_{\max}$ and $r_{\max}$ are the end-to-end length of the drop in the direction of electric field and the maximum breadth in the traverse direction, respectively. $\mathrm{Ca} = \mu_o u_s/\gamma$ is a capillary number, $u_s = \epsilon_o E_\infty^2 a/\mu_o$ is a velocity scale, and E_∞ is the unperturbed strength of the electric field. This equation suggests that $\mathcal{D}_\infty \sim E_\infty^2$ at low electric field strength, a fact that has been verified by various experimental and numerical studies [7].

While steady-state electrohydrodynamics of a liquid drop in a uniform electric field is reasonably well understood (see, for example, Ref. [8] and the references therein), not much is known about the fluid flow evolution toward the steady state and the deformation time history of a leaky dielectric drop. Such an understanding finds relevance in a host of microfluidic applications such as enhancement of mixing by electric forces [9], where information about the relative importance of the pertinent time scales of the phenomena compared to the time scale of the process of interest, and the manner in which the flow develops is a key to the optimum design and performance of the device. In what follows, we refer to a few studies that have focused on the transient dynamics and are particularly relevant to our work.

Sozou [10] was the first to investigate the evolution of the flow field in and around a leaky dielectric drop. He solved the creeping flow equations analytically, while retaining the local fluid acceleration term $\partial\mathbf{V}/\partial t$. He followed the evolution of the flow field for a case where $R < S$; however, he did not present the streamlines for the actual flow field; rather, he showed the flow fields due to the net electrical shear and normal stresses individually. For the shear-stress-driven flow and at an early

*esmaeeli@engr.siu.edu

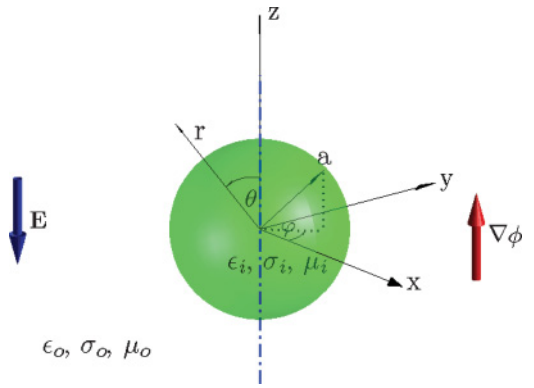

FIG. 1. (Color online) The geometric setup depicting a liquid drop surrounded by a pool of another liquid of infinite extension.

time, two sets of closed vortices were formed near the surface of the drop in each quadrant, inside and outside the drop. As time passed, the centers of the outer vortices gradually moved outward, pushing the outer fluid toward the drop surface and as a result, diminishing the inner vortices. This state of affairs continued until the drop deformation started to decelerate, whereby the inner vortices started to expand. The flow field eventually settled to the Taylor's steady-state result [1]. On the other hand, the flow driven by normal stresses at an early time showed only one set of vortices in each quadrant, with the streamlines that crossed the drop surface. The cores gradually moved outward, and the flow eventually diminished once the drop deformation reached a steady state. Since the authors did not present a closed-form solution, it was not possible to discern about the details of the evolution of the actual flow field and the deformation time history of the drop.

The deformation time history of a drop, $\mathcal{D}-t$, was found by Haywood *et al*. [11], who built on a quasi-steady state analysis developed by Moriya *et al*. [12] and a heuristic modification of the results of Ref. [12] by Nishiwaki *et al*. [13], and showed that $\mathcal{D}-t$ for a perfectly conducting liquid drop immersed in a perfect dielectric (PD) liquid is governed by $\mathcal{D}_{\mathrm{PD}} = \mathcal{D}_{\infty_{\mathrm{PD}}}[1 - \exp(-t/\tau)]$, where

$$\mathcal{D}_{\infty_{\mathrm{PD}}} = \frac{9\epsilon_o a E_\infty^2}{16\gamma} \tag{3}$$

is the steady-state deformation derived by Ref. [14] in the context of the electrostatic theory by determining the drop shape that minimizes the total energy, and $\tau = (\alpha\mu_i + \beta\mu_o)a/\gamma$ is the characteristic time; $\alpha = (38\widetilde{\mu} + 47)/(40\widetilde{\mu} + 40)$ and $\beta = (42\widetilde{\mu} + 48)/(40\widetilde{\mu} + 40)$ are the weighting functions. The authors reported excellent agreement between their numerical and analytical $\mathcal{D}-t$ for $\mathcal{D}_{\infty_{\mathrm{PD}}} \leqslant 0.025$ and $\mathrm{Oh} \geqslant 20$, $\mathrm{Oh} = \mu/\sqrt{\rho a\gamma}$ being the Ohnesorge number based on the properties of the outer fluid. Supeene *et al*. [15] performed numerical simulations using the commercial software package FEMLAB (COMSOL) and studied the transient deformation of a perfect dielectric liquid drop for several perfect dielectric fluid systems at low to moderate electric field strength. The deformation time history curves collapsed to a single curve for all the electric field strengths, once the deformation was scaled by the steady-state deformation predicted from the linear theory [14] and time was scaled by the natural frequency of oscillation of an inviscid drop in an AC electric field [16]. The deformation showed an oscillatory behavior, with a large initial peak that was followed by a couple of smaller dips and peaks as it settled to steady state. Supeene *et al*. [17] observed a similar behavior for leaky dielectric systems at low electric field strength.

The goal of this study is to present a simple closed-form solution for the transient dynamics of a leaky dielectric liquid drop under a uniform electric field of small strength and to investigate the contributions of the net normal and tangential electric stresses in the flow field and drop deformation. The "leaky dielectric framework" used here gives a realistic picture of the electrohydrodynamics of a drop (see Ref. [18] and the references therein), whereas the "perfect dielectric model" used by the authors of Ref. [11] will not do so in general. Briefly, the perfect dielectric model is based on the "electrostatic" theory, and as such it predicts that no fluid flow exists at steady state and that the drop would always deform to a prolate ellipsoid. Both of these predictions, however, have been ruled out by experiments (see, for example, Refs. [1,19]). The simple closed-form solution presented here makes it extremely easy to discern about the individual contribution of the electrical stresses in the various parameters of interest such as interfacial velocities. This is not the case with the solution of Sozou [10], while we acknowledge that Sozou's analysis was more general. Furthermore, the formalism introduced here provides a methodological basis for the study of this problem and the similar ones.

II. GOVERNING EQUATIONS AND THEIR SOLUTIONS

The problem setup is shown in Fig. 1, depicting a spherical coordinate system (r,θ,φ). Here the positive z axis is in the same direction as the electric potential gradient $\nabla\phi$, and since the problem is axisymmetric, the azimuth angle φ does not come to the picture. As shown by Refs. [2,20], for leaky dielectric fluids the electric field equation is decoupled from the momentum equation, however, the momentum equation is coupled to the electric field equation.

The electric field equation for both fluids is

$$\nabla^2\phi = 0, \tag{4}$$

where ϕ is the electric potential. This equation is the same as the one used by Ref. [1] and is derived from the charge conservation equation using the scaling arguments, which suggest that for leaky dielectric liquids, for small dynamic electrical currents, and in the absence of external magnetic field, the electric field intensity $\mathbf{E}$ is both irrotational, $\nabla\times\mathbf{E} = 0$, and divergence free, $\nabla\cdot\mathbf{E} = 0$. The first expression suggests that $\mathbf{E}$ can be written as a gradient of a scalar, $\mathbf{E} = -\nabla\phi$, and substitution for $\mathbf{E}$ in terms of ϕ in the second expression leads to Eq. (4).

The Navier-Stokes equation for both fluids is

$$\rho\left(\frac{\partial\mathbf{V}}{\partial t} + \mathbf{V}\cdot\nabla\mathbf{V}\right) = -\nabla P + \mu\nabla^2\mathbf{V}, \tag{5}$$

where we have used the usual notation. To account for the effect of electric field on the flow, an electric force density $\mathbf{F}_e$ [Nm^{-3}] should be generally added to the right-hand side of Eq. (5) as a body force. However, for leaky dielectric fluids with constant dielectric properties $\mathbf{F}_e$ is zero in the bulk and the contribution

of electric stresses appears only at the phase boundary, where these stresses are not zero (see, for example, Ref. [18]). To examine the appropriate form of the Navier-Stokes equation, we cast this equation in a nondimensional form, where we use $u_s = \epsilon E_\infty^2 a/\mu$ as the velocity scale, $l_s = a$ as the length scale, $t_s = \mu a/\gamma$ as the time scale, and $P_s = \mu u_s/a$ as the pressure scale to nondimensionalize the terms. Here u_s is constructed by balancing of the electric force and the viscous shear stress at the drop surface, and t_s is the process time of interest, which is the time required for relaxation of the drop to an equilibrium shape. This yields

$$\mathrm{Re}\left(\frac{1}{\mathrm{Ca}}\frac{\partial \mathbf{V}'}{\partial t'} + \mathbf{V}'\cdot\nabla'\mathbf{V}'\right) = -\nabla' P' + \nabla'^2\mathbf{V}', \qquad (6)$$

where primed variables are dimensionless, and $\mathrm{Re} = \rho u_s a/\mu$ and $\mathrm{Ca} = \mu u_s/\gamma$ are the Reynolds and capillary numbers, respectively. For sufficiently small electric field strength, $\mathrm{Re} \ll 1$, and, therefore, the convective term $\mathbf{V}\cdot\nabla\mathbf{V}$ can be ignored. If we further assume that $\mathrm{Re/Ca} \ll 1$, the inertia term $\partial\mathbf{V}/\partial t$ can also be ignored. Therefore, the Navier-Stokes equation reduces to $-\nabla P + \mu\nabla^2\mathbf{V} = 0$, which can be cast to a biharmonic equation for the streamfunction:

$$D^4\psi = 0, \qquad (7)$$

where $D^4 = D^2(D^2)$, and $D^2 = \partial^2/\partial r^2 + (\sin\theta/r^2)\{\partial/\partial\theta[(1/\sin\theta)\partial/\partial\theta]\}$ resembles the Laplacian. The velocities are related to the streamfunction through $u_r = [1/(r^2\sin\theta)](\partial\psi/\partial\theta)$ and $u_\theta = -[1/(r\sin\theta)](\partial\psi/\partial r)$.

We note that $\mathrm{Re/Ca} = \mathrm{Oh}^{-2}$, where $\mathrm{Oh} = \mu/\sqrt{\rho a\gamma}$ is the Ohnesorge number and that $\mathrm{Re/Ca} \ll 1$ implies that the time scale of momentum diffusion by viscosity $\tau_\mu = a^2/\nu$ is much smaller than the time scale of surface deformation $\tau_d = \mu a/\gamma$. In summary, using the properties of the ambient fluid, $\mathrm{Oh} = \mu_o/\sqrt{\rho_o a\gamma}$ and $\mathrm{Ca} = \epsilon_o E_\infty^2 a/\gamma$ are the primary nondimensional numbers of our problem, while $R = \sigma_i/\sigma_o$, $S = \epsilon_i/\epsilon_o$, and $\widetilde{\mu} = \mu_i/\mu_o$ provide us with a set of secondary nondimensional numbers.

There are two main differences between the current mathematical development and that of Ref. [1]; the phase boundary is assumed to be

$$\xi(t) = a[1 + (2/3)\mathcal{D}(t)(3\cos^2\theta - 1)], \qquad (8)$$

at the outset and also some of the interfacial jump conditions used to solve Eq. (7) will be different. The form of ξ is suggested by the (anticipated) form of the net normal electrical stresses. We note that variants of Eq. (8) have been used by others in *a posteriori* calculation of drop deformation [6] or to account for drop deformation *a priori* (see, for example, Refs. [10,21,22]). In particular, the authors of Ref. [6] used the same form of Eq. (8) to find steady state deformation of a drop (2) using Taylor's [1] solution. Here we assume that the drop deformation, $\mathcal{D}$, is very small (i.e., $\mathrm{Ca} \ll 1$); therefore, the interfacial jump conditions are imposed at $r = a$ rather than $r = \xi$. This assumption implies that the $r-\theta$ coordinates is a tangent-normal coordinate system; i.e., $r \equiv n$ and $\theta \equiv t$. Application of the boundary conditions at the undeformed surface has precedent in fluid flow analysis and has been done, for example, by Refs. [10,21,22], among others. The justification for doing so and the associated order of the error is discussed in Appendix A.

Equation (4) is decoupled from Eq. (7). However, Eq. (7) is coupled to Eq. (4) through the balances of the interfacial tangential and the normal stresses. Here the solution of Eq. (4) is the same as that of Ref. [1], and therefore the jump in the normal electrical stresses

$$[\![\tau_{rr}^e]\!] = \frac{9\epsilon_o E_\infty^2}{2(R+2)^2}[(R^2+1-2S)\cos^2\theta + S - 1] \qquad (9)$$

and the tangential electrical stresses

$$[\![\tau_{r\theta}^e]\!] = \frac{9\epsilon_o E_\infty^2}{2(R+2)^2}(S-R)\sin 2\theta \qquad (10)$$

remain the same, where the jump in a physical quantity such as Q across the interface is defined as $[\![Q]\!] = Q_o - Q_i$. Note that in Eqs. (9) and (10) Taylor's [1] results have been transformed to the notations used in Ref. [18] and here.

To solve Eq. (7), the following eight boundary conditions are used: (1) u_{r_i} and u_{θ_i} should be bounded at $r = 0$, (2) $u_{\theta_o} = u_{\theta_i}$ at $r = a$, (3) $u_{r_o} = u_{r_i} = d\xi/dt$ at $r = a$, (4) $[\![\tau_{r\theta}^h]\!] + [\![\tau_{r\theta}^e]\!] = 0$, (5) $-[\![P]\!] + [\![\tau_{rr}^h]\!] + [\![\tau_{rr}^e]\!] = \gamma\kappa$, and (6) $u_{r_o}, u_{\theta_o} \sim 0$, as $r \to \infty$. Notice that the boundary conditions 1, 3, and 6 each provides two boundary conditions. In the above equations, κ is twice the mean curvature of the drop and $[\![\tau_{r\theta}^h]\!]$ and $[\![\tau_{rr}^h]\!]$ are jump in the tangential and normal stresses, respectively.

Boundary condition 4 suggests a solution of the form $\psi(r,\theta) = r^n\sin^2\theta\cos\theta$ for Eq. (7), where n is a real constant to be determined. Substitution for ψ using this expression into Eq. (7) results in an algebraic equation for n, the solution of which leads to $n = 0$, -2, 3, and 5. This yields $\psi_o = (A + Br^{-2} + Cr^3 + Dr^5)\sin^2\theta\cos\theta$ and $\psi_i = (E + Fr^{-2} + Gr^3 + Hr^5)\sin^2\theta\cos\theta$, where A–H are constants to be determined. Application of boundary conditions 1 and 6 results in $E = G = 0$, $C = D = 0$, respectively. Therefore,

$$\psi_o = (Br^{-2} + A)\sin^2\theta\cos\theta \qquad (11)$$

and

$$\psi_i = (Fr^3 + Hr^5)\sin^2\theta\cos\theta. \qquad (12)$$

Before the application of the rest of the boundary conditions, we need to compute κ, $[\![P]\!]$, $[\![\tau_{rr}^h]\!]$, and $[\![\tau_{r\theta}^h]\!]$. Curvature is calculated from Eq. (B4) (see Appendix B for details), and to find $[\![P]\!]$, the velocity fields are computed from the streamfunctions and are supplied to the momentum equation $\nabla P = \mu\nabla^2\mathbf{V}$, which is then integrated in terms of the pressure. This results in

$$[\![P]\!] = (2\mu_o A a^{-3} - 7\mu_i H a^2)(3\cos^2\theta - 1) + \Pi_o - \Pi_i, \qquad (13)$$

where Π_o and Π_i are the integration constants. Similarly, the jump in hydrodynamic stresses are found by computing their pertinent terms using the velocity fields:

$$[\![\tau_{rr}^h]\!] = [2\mu_o(-2Aa^{-2} - 4Ba^{-5}) - 2\mu_i(F + 3Ha^2)] \times (3\cos^2\theta - 1) \qquad (14)$$

and

$$[\![\tau_{r\theta}^h]\!] = [\mu_o(-8Ba^{-5} - 3Aa^{-3}) - \mu_i(-8Ha^2 - 3F)] \times \sin 2\theta. \qquad (15)$$

Application of boundary conditions 2, 3, 4, and 5, respectively, results in

$$3Fa + 5Ha^3 + 2Ba^{-4} = 0, \tag{16}$$

$$F + Ha^2 = \frac{2}{3}\frac{d\mathcal{D}}{dt}, \tag{17}$$

$$Aa^{-2} + Ba^{-4} = \frac{2}{3}a\frac{d\mathcal{D}}{dt}, \tag{18}$$

$$-6\mu_o a^{-3}A - 16\mu_o a^{-5}B + 16\mu_i a^2 H + 6\mu_i F + \frac{9\epsilon_o E_\infty^2 (S-R)}{(R+2)^2} = 0, \tag{19}$$

and

$$-18\mu_o a^{-3}A - 24\mu_o a^{-5}B - 6\mu_i F + 3\mu_i a^2 H + \frac{9\epsilon_o E_\infty^2}{2(R+2)^2}(R^2+1-2S) = \frac{8\gamma\mathcal{D}}{a}. \tag{20}$$

Notice that since the jump conditions should be valid at any point at the drop surface, only the coefficients of $\cos^2\theta$ terms in the normal stress balance are retained. Equations (16)–(20) constitute five equations for the unknowns A, B, F, H, and $\mathcal{D}$. Evaluation of A, B, F, and H in terms of $\mathcal{D}$ from Eqs. (16)–(19) and substitution in Eq. (20) results in

$$\tau\frac{d\mathcal{D}}{dt} + \mathcal{D} - \mathcal{D}_\infty = 0, \tag{21}$$

where

$$\tau = \frac{a\mu_o}{\gamma}\frac{(19\widetilde{\mu}+16)(2\widetilde{\mu}+3)}{40(\widetilde{\mu}+1)}, \tag{22}$$

τ is the time scale that governs the dynamics, $\mathcal{D}_\infty$ is the steady-state deformation defined earlier (2), $\mathrm{Ca} = \mu_o u_s/\gamma$, and $u_s = \epsilon_o E_\infty^2 a/\mu_o$. Solution of Eq. (21) results in the deformation time history

$$\mathcal{D} = \mathcal{D}_\infty[1 - \exp(-t/\tau)], \tag{23}$$

which suggests that the drop deformation settles monotonically to its steady-state value. Having found $\mathcal{D}$, the rest of unknowns are readily determined:

$$A = -U_{\max}a^2 + \frac{3}{2}\left[\frac{u_s a^2}{(R+2)^2}\right]\left[\frac{1}{2\widetilde{\mu}+3}\right] \times \Phi\exp(-t/\tau), \tag{24}$$

$$B = U_{\max}a^4 - \frac{9}{2}\left[\frac{u_s a^4}{(R+2)^2}\right]\left[\frac{3\widetilde{\mu}+2}{(19\widetilde{\mu}+16)(2\widetilde{\mu}+3)}\right] \times \Phi\exp(-t/\tau), \tag{25}$$

$$F = \frac{U_{\max}}{a} + \frac{3}{2}\left[\frac{u_s}{(R+2)^2 a}\right]\left[\frac{16\widetilde{\mu}+19}{(19\widetilde{\mu}+16)(2\widetilde{\mu}+3)}\right] \times \Phi\exp(-t/\tau), \tag{26}$$

and

$$H = -\frac{U_{\max}}{a^3} - \frac{9}{2}\left[\frac{u_s}{(R+2)^2 a^3}\right]\left[\frac{1}{19\widetilde{\mu}+16}\right]\Phi\exp(-t/\tau), \tag{27}$$

where

$$U_{\max} = \frac{9u_s(S-R)}{10(\widetilde{\mu}+1)(R+2)^2} \tag{28}$$

is the maximum surface velocity.

A few comments about this solution are in order. In the limit of $t \to \infty$, the solution is the same as that of Ref. [1]. The deformation depends on the capillary number and to the lesser extent the viscosity ratio. The characteristic time τ is the same as the one derived by Ref. [11] for a perfectly conducting drop immersed in a perfect dielectric liquid and is also the same as the relaxation time of a liquid drop in a general linear flow (see, for example, Refs. [23,24]). This is because the restoring forces in all of these problem are all the same, regardless of the driving forces that are different. For a relatively inviscid drop ($\widetilde{\mu} \ll 1$), τ is controlled by the viscosity of the external flow μ_o. On the other hand, for a drop that is much more viscous than the ambient ($\widetilde{\mu} \gg 1$), τ is controlled by the viscosity of the drop μ_i. Here τ is independent of the electric field strength as E_∞ is assumed to be sufficiently small. We note that our solution will converge to that of Ref. [11] if we set $R = S$ (i.e., perfect dielectric model) and evaluate the terms in Eqs. (24)–(27) when $S \to \infty$ (i.e., a perfectly conducting drop). Setting $R = S$ results in $U_{\max} = 0$, which implies that no fluid flow will exist at steady state, and taking the limit of $\mathcal{D}_\infty$ (2) when $S \to \infty$ will lead to $\mathcal{D}_{\infty_{\mathrm{PD}}}$ (3). This suggests that the drop will always deform to a prolate, as $\mathcal{D}_{\infty_{\mathrm{PD}}}$ is always positive.

In passing, we point out that the decomposition used by Ref. [11] (i.e., values of α and β used in their formulation for τ) is quite arbitrary. To see this, one can rewrite their $\tau = (\alpha\mu_i + \beta\mu_o)a/\gamma$ in a slightly different form by substitution for $\widetilde{\mu} = \mu_i/\mu_o$. This yields

$$\tau = \frac{[\mu_i(38\mu_i + 47\mu_o) + \mu_o(42\mu_i + 48\mu_o)]a}{40\gamma(\mu_i + \mu_o)},$$

where the term in the bracket can be simplified to $Q = 38\mu_i^2 + 89\mu_i\mu_o + 48\mu_o^2$. The characteristic time τ can be decomposed in many different ways according to the decomposition of Q. For instance, if $Q = \mu_i(38\mu_i + 32\mu_o) + \mu_o(57\mu_i + 48\mu_o)$, then $\alpha = (38\widetilde{\mu}+32)/(40\widetilde{\mu}+40)$ and $\beta = (57\widetilde{\mu}+48)/(40\widetilde{\mu}+40)$, which is different than the weighting functions that they used.

Detailed understanding of the individual contribution of the net normal and tangential electric stresses ($[\![\tau_{rr}^e]\!]$ and $[\![\tau_{r\theta}^e]\!]$, respectively) in the dynamic is very insightful, since these stresses are the driving forces behind the fluid flow and the drop deformation. To evaluate the individual contribution of $[\![\tau_{r\theta}^e]\!]$, we set $[\![\tau_{rr}^e]\!] = 0$ in boundary condition 5 and solve Eq. (7) with the rest of the boundary conditions intact. To do so, we consider a solution of the form $\psi_{o_t} = (B_t r^{-2} + A_t)\sin^2\theta\cos\theta$ and $\psi_{i_t} = (F_t r^3 + H_t r^5)\sin^2\theta\cos\theta$, where subscript t refers to the fact the flow is solely driven by the net tangential electrical stresses. Setting $[\![\tau_{rr}^e]\!] = 0$ is tantamount to setting $E_\infty = 0$ in the last term of Eq. (20) as this term is the θ-dependent part of $[\![\tau_{rr}^e]\!]$ according to Eq. (9). We then solve Eqs. (16)–(19) along with the modified Eq. (20), and unknowns A, B, F, H, and $\mathcal{D}$ replaced by A_t, B_t, F_t, H_t, and $\mathcal{D}_t$, respectively. This yields

$$\mathcal{D}_t = \mathcal{D}_{\infty_t}[1 - \exp(-t/\tau)], \tag{29}$$

$$\mathcal{D}_{\infty_t} = \frac{9\mathrm{Ca}}{16}\frac{\Phi_t}{(R+2)^2}, \tag{30}$$

TABLE I. Physical properties of the fluids used. Here $\gamma = 5.5 \times 10^{-3}$ [Nm^{-1}] and $\epsilon_0 = 8.854 \times 10^{-12}$ [Fm^{-1}]. Systems *A* and *B* correspond, respectively, to a silicon oil drop surrounded by oxidized castor oil and the phase-reversed system. System *A* corresponds to system (17) of Ref. [22].

Fluid	σ [Sm^{-1}]	ϵ [Fm^{-1}]	μ [kg m^{-1} s^{-1}]	ρ [kg m^{-3}]
Silicon oil	3.33×10^{-11}	$2.77\ \epsilon_0$	12	980
Oxidized castor oil	1.11×10^{-12}	$6.3\ \epsilon_0$	6.5	980

$$A_t = -U_{\max} a^2 + \frac{3}{2}\left[\frac{u_s a^2}{(R+2)^2}\right]\left[\frac{1}{2\widetilde{\mu}+3}\right]\Phi_t \exp(-t/\tau), \tag{31}$$

$$B_t = U_{\max} a^4 - \frac{9}{2}\left[\frac{u_s a^4}{(R+2)^2}\right]\left[\frac{3\widetilde{\mu}+2}{(19\widetilde{\mu}+16)(2\widetilde{\mu}+3)}\right] \times \Phi_t \exp(-t/\tau), \tag{32}$$

$$F_t = \frac{U_{\max}}{a} + \frac{3}{2}\left[\frac{u_s}{(R+2)^2 a}\right]\left[\frac{16\widetilde{\mu}+19}{(19\widetilde{\mu}+16)(2\widetilde{\mu}+3)}\right] \times \Phi_t \exp(-t/\tau), \tag{33}$$

and

$$H_t = -\frac{U_{\max}}{a^3} - \frac{9}{2}\left[\frac{u_s}{(R+2)^2 a^3}\right]\left[\frac{1}{19\widetilde{\mu}+16}\right]\Phi_t \exp(-t/\tau), \tag{34}$$

where

$$\Phi_t = R - S. \tag{35}$$

To determine the contribution of $[\![\tau^e_{rr}]\!]$, we consider

$$\mathcal{D}_n = \mathcal{D}_{\infty_n}[1 - \exp(-t/\tau)], \tag{36}$$

$\psi_{o_n} = (B_n r^{-2} + A_n)\sin^2\theta\cos\theta$, and $\psi_{i_n} = (F_n r^3 + H_n r^5)\sin^2\theta\cos\theta$. However, since the problem is linear, $\mathcal{D}_n$, A_n, B_n, F_n, and H_n can be readily determined by subtracting $\mathcal{D}_t$, A_t, B_t, F_t, and H_t from $\mathcal{D}$, A, B, F, and H, respectively. This yields

$$\mathcal{D}_{\infty_n} = \frac{9\mathrm{Ca}}{16}\frac{\Phi_n}{(R+2)^2}, \tag{37}$$

$$A_n = \frac{3}{2}\left[\frac{u_s a^2}{(R+2)^2}\right]\left[\frac{1}{2\widetilde{\mu}+3}\right]\Phi_n \exp(-t/\tau), \tag{38}$$

$$B_n = -\frac{9}{2}\left[\frac{u_s a^4}{(R+2)^2}\right]\left[\frac{3\widetilde{\mu}+2}{(19\widetilde{\mu}+16)(2\widetilde{\mu}+3)}\right]\Phi_n \exp(-t/\tau), \tag{39}$$

$$F_n = \frac{3}{2}\left[\frac{u_s}{(R+2)^2 a}\right]\left[\frac{16\widetilde{\mu}+19}{(19\widetilde{\mu}+16)(2\widetilde{\mu}+3)}\right]\Phi_n \exp(-t/\tau), \tag{40}$$

and

$$H_n = -\frac{9}{2}\left[\frac{u_s}{(R+2)^2 a^3}\right]\left[\frac{1}{19\widetilde{\mu}+16}\right]\Phi_n \exp(-t/\tau), \tag{41}$$

where

$$\Phi_n = R^2 + 1 - R - S + \frac{3}{5}(R-S)\frac{3\widetilde{\mu}+2}{\widetilde{\mu}+1}. \tag{42}$$

III. RESULTS AND DISCUSSION

To investigate the transient electrohydrodynamics of leaky dielectric drops, we consider two fluid systems, a system where the drop fluid is less conductive than the surrounding fluid (i.e., $R < 1$ and $R < S$), and a phase-reversed system (i.e., $R > 1$ and $R > S$). The first system consists of a silicon oil drop of radius $a = 10$ [mm], surrounded by an oxidized castor oil, and exposed to an electric field of strength $E_\infty = 10$ [kV/m]. The fluid properties in this fluid system correspond to those of system (17) of Ref. [22] and are listed in Table I. Here the resulting nondimensional numbers are $\mathrm{Oh} = 51.69$, $\mathrm{Ca} = 0.0187$, $R = 0.033$, $S = 2.27$, $\widetilde{\rho} = 1$, and $\widetilde{\mu} = 0.542$. Figure 2 shows a few equispaced streamlines contours at an early time ($t/\tau = 0.001$), an intermediate time ($t/\tau = 2$), and a steady state ($t/\tau = 5$). At the early time, the flow consists of four open vortices in each quadrant, and the direction of the flow is from the poles to the equator. The streamlines cross the interface, reflecting the fact that the drop surface is deforming (frame 1). As time passes, the flow retreats outside and the streamlines open up, leaving behind four vortices inside the drop (frame 2). The drop surface is still deforming as is evidenced from a set of streamlines that cross the interface. The inner vortices become stronger as the time passes, and at steady state they occupy the inner space (frame 3). The coordinates of the cores of the inner vortices can be determined by finding the points where both u_r and u_θ are zero. This results in $\theta_c = \pm 0.9553$, ± 2.5261 and $r_c = \sqrt{-3F/5H}$, which suggests that the angular positions of the vortices are fixed, but their radial positions change with the time. Note that r_c is only acceptable if it is real and $0 < r_c \leqslant a$. The cores initially appear at $r_c \sim 0.34a$ and gradually shift to $r_c \sim 0.77a$.

To explore the contribution of the electrical stresses in the structure of the flow field, in Fig. 3 we compare the flow due to $[\![\tau^e_{r\theta}]\!]$ (left frame) and $[\![\tau^e_{rr}]\!]$ (right frame), corresponding to the middle frame of Fig. 2. This figure clearly shows that the net electrical shear stresses are solely responsible for the formation of the inner vortices. Notice that the flow strengths cannot be discerned from the figure as the information about the level contours are not given. While the general features of the flow as depicted here are similar to that of Ref. [10], the evolution of the two flows is not exactly the same. Here the flow is established impulsively since we assume $\tau_\mu = a^2/\nu \ll \tau_d = \mu a/\gamma$. This is not the case for Ref. [10], which considers τ_μ and τ_d to be of the same order.

To examine the contribution of $[\![\tau^e_{rr}]\!]$ and $[\![\tau^e_{r\theta}]\!]$ to the degree of deformation and the strength of the flow field, in Fig. 4 we plot $\mathcal{D}$, $u_{r_{\max}} = u_r(a,0)$, and $u_{\theta_{\max}} = u_\theta(a,\pi/4)$ as a function of time. For this fluid system, $\Phi = -6.6951 < 0$ and therefore, $\mathcal{D} < 0$, which implies that the drop becomes oblate.

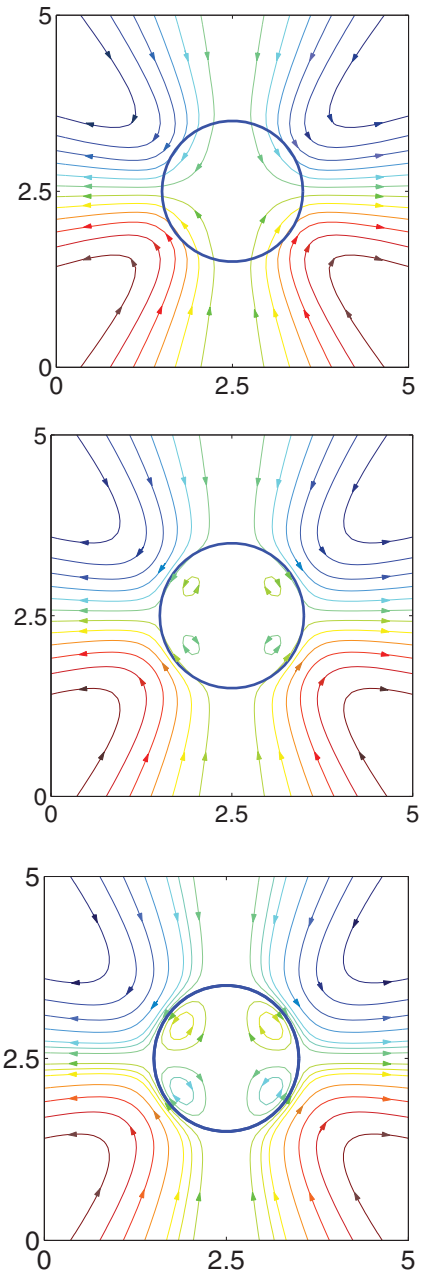

FIG. 2. (Color online) Evolution of velocity streamlines for a silicon oil drop in an oxidized castor oil. The nondimensional numbers are Oh = 51.69, Ca = 0.0187, $R = 0.033$, $S = 2.27$, $\widetilde{\rho} = 1$, and $\widetilde{\mu} = 0.542$. The times are $\widetilde{t} = 0.001$, 2, and 5, respectively, and proceed from the top to the bottom. Here the fluid inside is less conductive than the fluid outside (i.e., $R < 1$, $R < S$), and the ambient fluid flows from the poles to the equator.

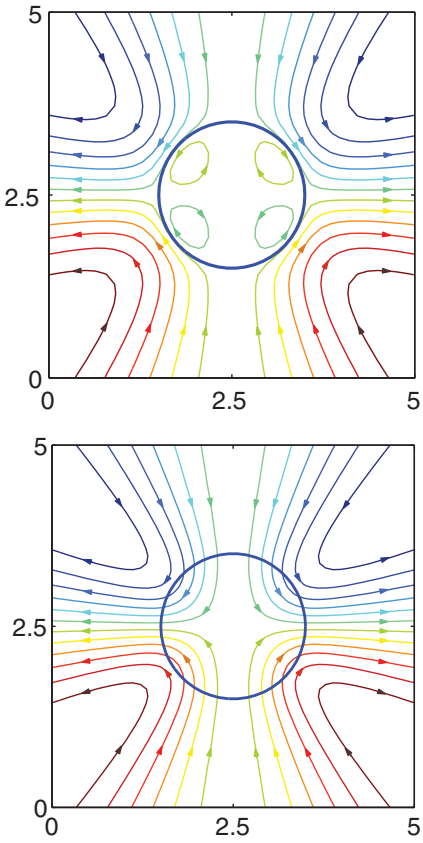

FIG. 3. (Color online) Streamline contours for the flow driven by $[\![\tau^e_{r\theta}]\!]$ (left frame) and $[\![\tau^e_{rr}]\!]$ (right frame), corresponding to the middle frame of Fig. 2.

Here $|\mathcal{D}_n| > |\mathcal{D}_t|$, but $|\mathcal{D}_n|$ and $|\mathcal{D}_t|$ are of the same order, which suggests that the contributions of $[\![\tau^e_{rr}]\!]$ and $[\![\tau^e_{r\theta}]\!]$ in the interface deformation are of the same order. This is because the main difference between $\mathcal{D}_t$ and $\mathcal{D}_n$, as given by Eqs. (37) and (30), lies in the difference between Φ_t and Φ_n. For this fluid system, however, $\Phi_t = -2.2370$ and $\Phi_n = -4.4581$, which are of the same order. Inspection of Eqs. (31)–(34) shows that the contribution of $[\![\tau^e_{r\theta}]\!]$ in the fluid flow is through the hydrodynamic shear stresses (the first term that is proportional to $U_{\max}$) as well as the instantaneous motion of the interface (the unsteady term). This can be clearly seen from Fig. 4, which shows that as the interface deformation stops at steady state, u_{r_t}, which is due to the interface deformation, settle to zero, however, u_{θ_t}, which originates from the hydrodynamic shear stresses, settles to a nonzero value. On the other hand, inspection of Eqs. (38)–(41) shows that the contribution of $[\![\tau^e_{rr}]\!]$ in the fluid flow is solely through the instantaneous motion of the interface (the unsteady term). This can be clearly seen from Fig. 4, where both u_{r_n} and u_{θ_n} settle to zero at steady state as the interface ceases to move.

Figure 5 shows a few equispaced streamlines contours for the phase-reversed system (i.e., oxidized castor oil in corn oil) at an early time ($t/\tau = 0.001$), an intermediate time ($t/\tau = 4.5$), and a steady state ($t/\tau = 10$). Note that the drop radius and the electric field strength remain the same as before. Here, the nondimensional numbers are Oh = 28, Ca = 0.0101, $R = 30$, $S = 0.44$, $\widetilde{\rho} = 1$, and $\widetilde{\mu} = 1.846$. Compared to the first system, the overall shape of the streamline contours is very much similar; however, the flow directions are opposite; i.e., whereas the outer flow in Fig. 2 was from the poles to the equator, here the direction is reversed. Similarly, the directions of the corresponding inner vortices of the two figures are opposite. Figure 6 shows $\mathcal{D}$, $u_{r_{\max}}$, and $u_{\theta_{\max}}$ versus time. Here as opposed to the first system, $\Phi = 947.096$ and therefore, $\mathcal{D} > 0$, which implies that the interface becomes prolate. Furthermore, the contribution of

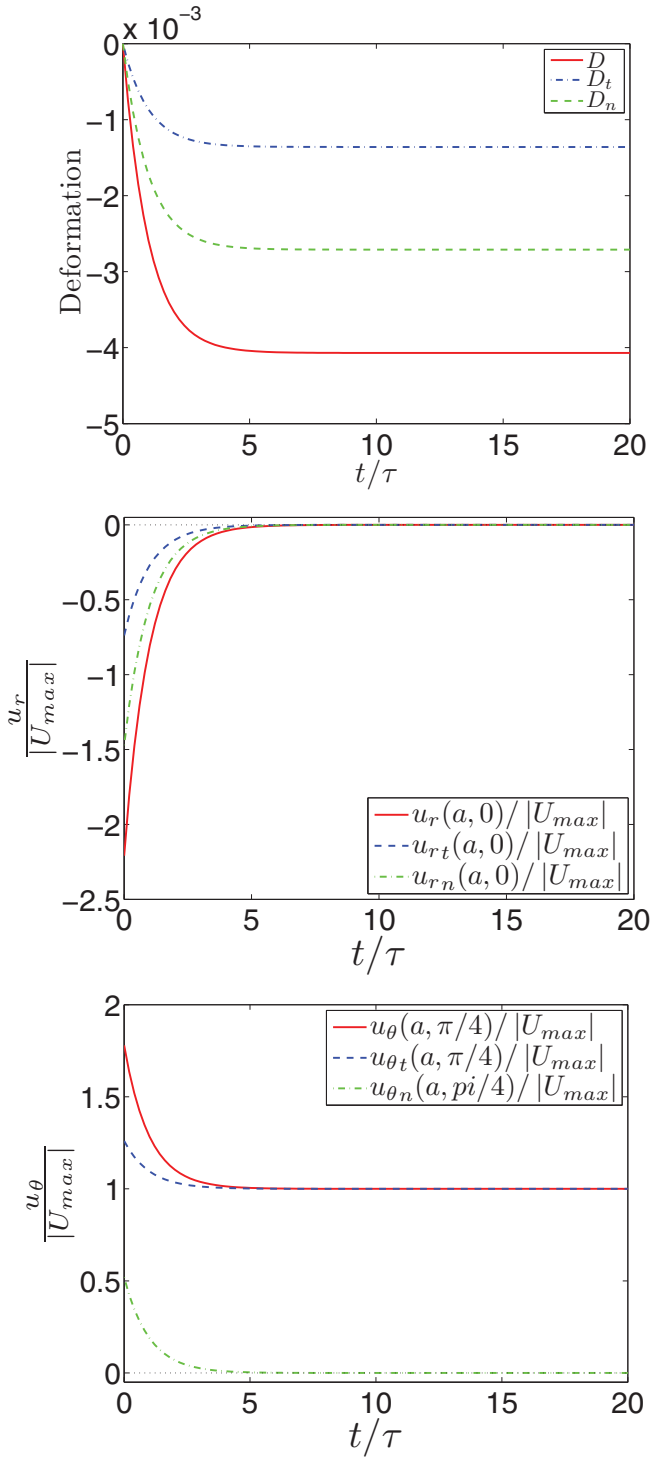

FIG. 4. (Color online) Deformation time history of the drop (top frame) and the evolutions of the radial (middle frame) and tangential (bottom frame) interfacial velocities. The frames correspond to the fluid system of Fig. 2.

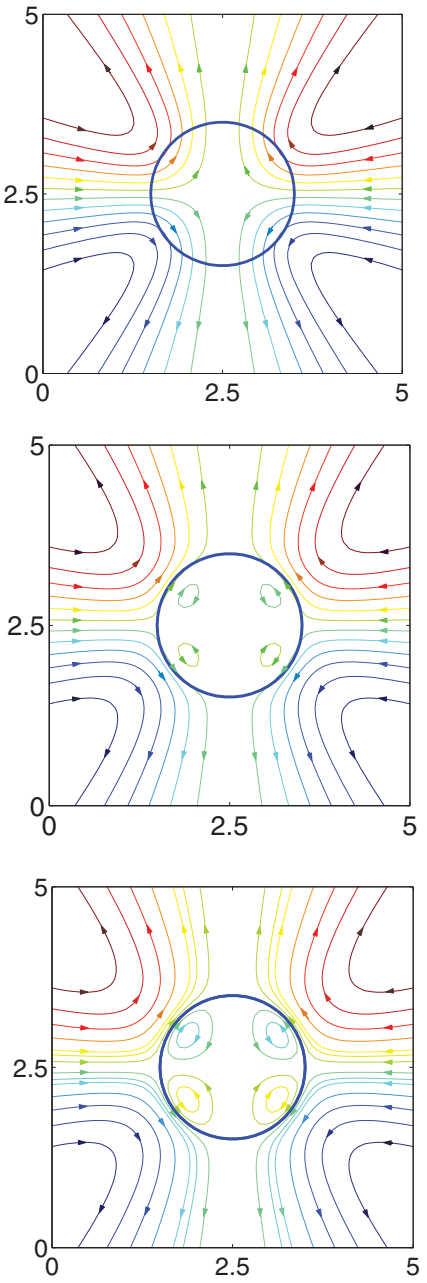

FIG. 5. (Color online) Evolution of velocity streamlines for an oxidized castor oil drop in a silicon oil. The nondimensional numbers are Oh = 28, Ca = 0.0101, $R = 30$, $S = 0.44$, $\widetilde{\rho} = 1$, and $\widetilde{\mu} = 1.846$. The times are $\widetilde{t} = 0.001$, 4.5, and 10, respectively, and proceed from the top to the bottom. Here the fluid inside is more conducting than the fluid outside (i.e., $R > 1$, $R > S$), and the ambient fluid flows from the equator to the poles.

$[\![\tau^e_{r\theta}]\!]$ in the deformation is negligible as $\Phi_t = 29.56$ is much smaller than $\Phi_n = 917.536$. Similar to the first system, $|u_{r_n}|$ is larger than $|u_{r_t}|$; however, now the difference between the two velocities (during the transient) are much larger because of the much larger difference between $\mathcal{D}_n$ and $\mathcal{D}_t$. Interestingly, $|u_{\theta_n}|$ is much larger than $|u_{\theta_t}|$ during the transient, which is due to the large difference in Φ_n and Φ_t. However, as before, u_{θ_n} settles to zero at steady state as the drop deformation stops.

In the two case that was just described, the directions of the streamlines in the ambient fluid implies that the fluid tends to deform the drop to an oblate ellipsoid in the first system while it tends to deform it to a prolate one in the second system. While this is exactly what happened, this observation should not be treated as a general rule. The tendency of the fluid flow to deform the drop in a certain direction is not the only factor that

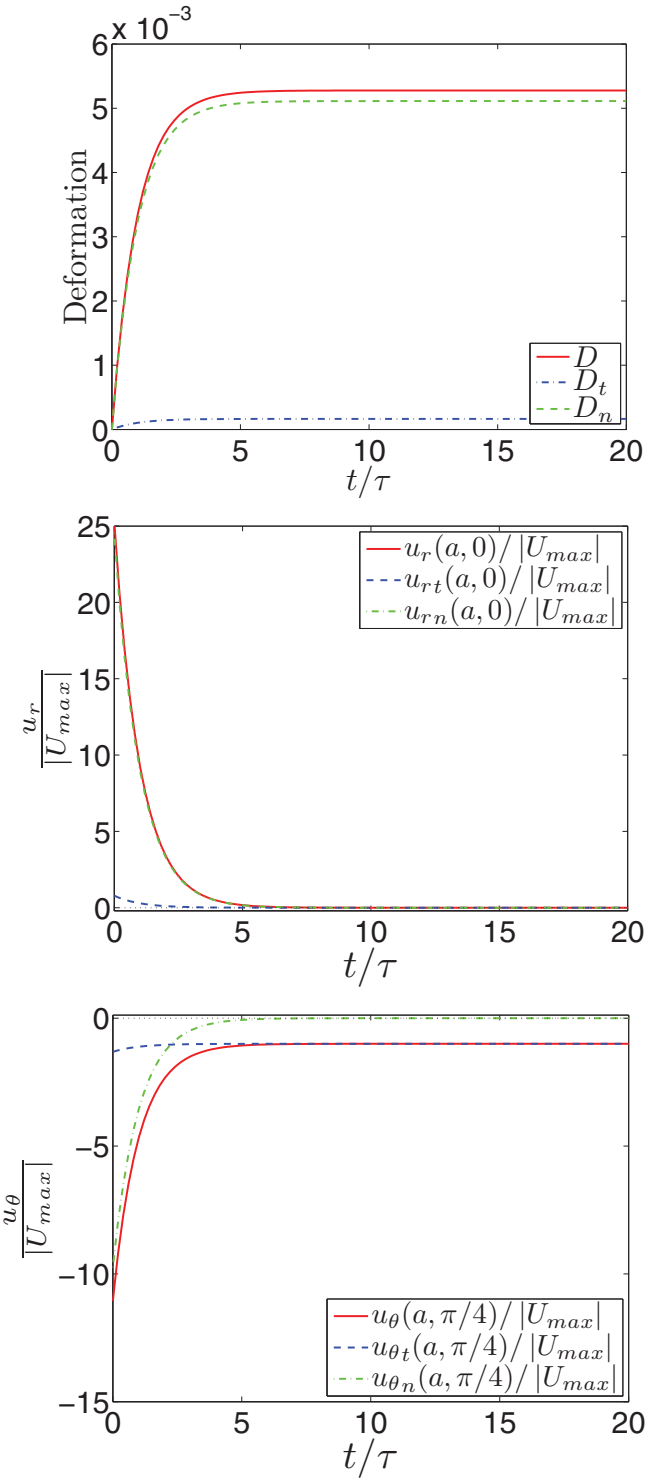

FIG. 6. (Color online) Deformation time history of the drop (top frame) and the evolutions of the radial (middle frame) and tangential (bottom frame) interfacial velocities. The frames correspond to the fluid system of Fig. 5.

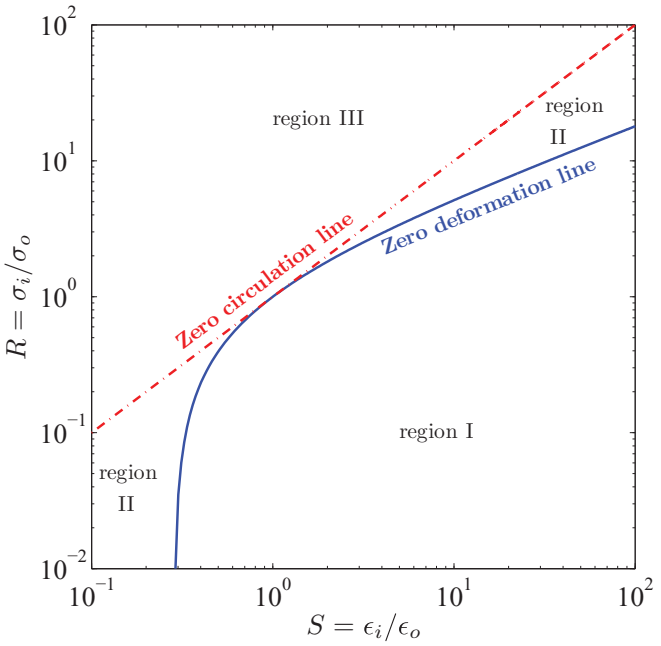

FIG. 7. (Color online) Circulation-deformation map. In region I, $R < S$ and $\Phi < 0$, the drop deforms to an oblate, and the flow is from the poles to the equator. In region II, $R < S$ and $\Phi > 0$, the drop deforms to a prolate, and the flow is still from the poles to the equator. In region III, $R > S$ and $\Phi > 0$ the drop deforms to a prolate, and the flow is from the equator to the poles.

determines the sense of deformation, rather, it is the balance of the normal stresses that does so. To characterize the effect of fluid flow on the sense of drop deformation in general, we construct a circulation-deformation map in $S - R$ coordinates following Refs. [18,22,25]. From Eqs. (1), (2), and (28) it is seen that the senses of flow circulation and deformation are determined by the signs of $S - R$ and Φ, respectively. Thus, we plot the $\Phi = 0$ curve and $R = S$ line together in $S - R$ coordinates. Notice that since Φ is a weak function of $\widetilde{\mu}$, $\Phi = 0$ is plotted only for $\widetilde{\mu} = 1$. The $R = S$ line and $\Phi = 0$ curve divide the parameter space into three regions (Fig. 7). In region I, $R < S$ and $\Phi < 0$; therefore, the drop will be deformed to an oblate, and the flow will be from the poles to the equator. In region II, $R < S$ and $\Phi > 0$; therefore, the drop will be deformed to a prolate and the flow will be still from the poles to the equator. In region III, $R > S$ and $\Phi > 0$; therefore, the drop will be deformed to a prolate, and the flow will be from the equator to the poles. This suggests that for fluid systems where $R \geqslant S$, the drop would always deform to a prolate, while for fluid systems where $R < S$, the drop would either deform to a prolate or an oblate. For the two fluid systems considered here, the signs of Φ_n and Φ_t were the same, which implied that the net normal and tangential electric stresses tended to deform the drop in the same direction. This is not true in general as we can easily envision a case where Φ_n and Φ_t have opposite signs. Indeed, if the curve $\Phi_n = 0$ is added to Fig. 7 and the line $R = S$ is treated as $\Phi_t = 0$ line, the parameter space will be divided into five regions according to the signs of Φ_n, Φ_t, and Φ (Fig. 8). In region I, $\Phi_t < 0$, $\Phi_n < 0$, and $\Phi < 0$; in region II, $\Phi_t < 0$, $\Phi_n > 0$, and $\Phi < 0$; in region III, $\Phi_t < 0$, $\Phi_n > 0$, and $\Phi > 0$; in region IV, $\Phi_t > 0$, $\Phi_n > 0$, and $\Phi > 0$; and in region V, $\Phi_t < 0$, $\Phi_n > 0$, and $\Phi > 0$. Note that region II is the narrow region enclosed by $\Phi = 0$ and $\Phi_n = 0$ curves and is identified by the diamond symbols. As is evident, in regions II, III, and V the senses of the deformation induced by

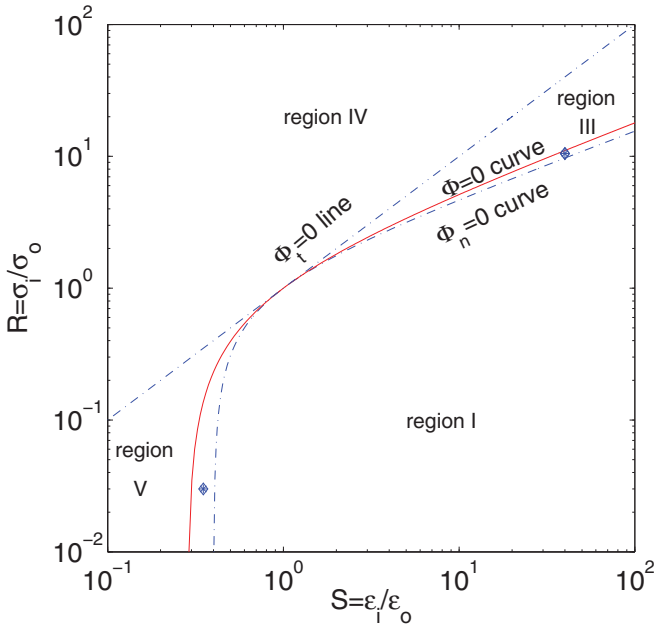

FIG. 8. (Color online) Deformation map according to the components of the electrical stresses. In region I, $\Phi_t < 0$, $\Phi_n < 0$, and $\Phi < 0$; in region II, $\Phi_t < 0$, $\Phi_n > 0$, and $\Phi < 0$; in region III, $\Phi_t < 0$, $\Phi_n > 0$, and $\Phi > 0$; in region IV, $\Phi_t > 0$, $\Phi_n > 0$, and $\Phi > 0$; and in region V, $\Phi_t < 0$, $\Phi_n > 0$, and $\Phi > 0$. Region II is the narrow region enclosed by $\Phi = 0$ and $\Phi_n = 0$ curves and is identified by the diamond symbols.

the net normal and tangential electrical stresses are opposite, while they are the same for regions I and IV.

We note that the sense of drop deformation is determined not only by the local direction (i.e., inward versus outward) of the sum of the net normal electric and hydrodynamic stresses, $[\![\tau^e_{rr}]\!] + [\![\tau^h_{rr}]\!]$, but also by the variations of these stresses at the drop surface. For instance, for perfect dielectric fluids ($R = S$) the hydrodynamic stresses vanish at steady state (i.e., $[\![\tau^h_{rr}]\!] = [\![\tau^h_{r\theta}]\!] = 0$), as the net tangential electrical stresses are zero according to Eq. (10). As a result, the deformation of these systems are solely determined by the net normal electric stresses. Furthermore, for these fluid systems it is known that the net normal electric stresses are directed from the fluid of higher electric permittivity toward the one with lower permittivity, i.e., $[\![\tau^e_{rr}]\!] > 0$ for $S > 1$ and $[\![\tau^e_{rr}]\!] < 0$ for $S < 1$. However, for both $S > 1$ and $S < 1$ cases the drop deforms always to a prolate [18]. As an example, consider two perfect dielectric systems (i.e., $R = S$) with $S = 2$ and $S = 0.5$. The terms in the bracket in Eq. (9), which represent the distribution of $[\![\tau^e_{rr}]\!]$, are $[1 + \cos^2\theta]$ and $[-0.5 + 0.25\cos^2\theta]$ for the first and the second systems, respectively. For the first system, the net stresses point outward with their maxima at the poles and minima at the equator, while for the second system the net stresses are inward with their minima at the poles and maxima at the equator. However, it can be easily envisioned that the net results in both cases is the deformation of the drop to a prolate ellipsoid.

The analysis so far was based on the premise that the viscous time scale $t_\mu = a^2/\nu$ is vanishingly small. As a result, the flow started impulsively and the evolution of the flow from the quiescent state could not be captured here. Furthermore, the drop deformation and the velocity developed monotonically toward the steady state. The fluid inertia can be of importance in a class of problems where $\tau_\mu = a^2/\nu$ is still less than $\tau_d = \mu a/\gamma$ but it cannot be ignored. For this class of problems, we conjecture that the phenomenon will be governed by two time scales, i.e., τ_μ and τ_d. Here the velocity field (characterized, for example, by the average kinetic energy of the fluids) would evolve from the quiescent state to a local peak in a time interval that is of the order of t_μ and then gradually would settle to a steady state. For the small deformation considered here, the drop deformation would still monotonically settle to its steady-state value in a time interval of the order of τ_d. For larger deformations, the dynamics becomes more complex, and both the deformation and the velocity field might settle to their steady-state values in a nonmonotonic way. The numerical simulations of Ref. [26] lend some support to these arguments.

IV. CONCLUSIONS

The transient dynamics of a liquid drop surrounded by another liquid and driven by a uniform electric field was investigated analytically. It was shown that for small distortion from a spherical shape and for large Ohnesorge number, the deformation time history is $\mathcal{D} = \mathcal{D}_\infty[1 - \exp(-t/\tau)]$, where $\tau = (a\mu_o/\gamma)(19\widetilde{\mu} + 16)(2\widetilde{\mu} + 3)/(40\widetilde{\mu} + 40)$ is the characteristic time scale. The contributions of the net normal and tangential electric stresses in the degree of deformation and fluid flow strength and structure were determined, and it was shown that the former contributes to the fluid flow through the instantaneous motion of the phase boundary while the latter contributes through that effect as well as creation of the net hydrodynamic shear stresses. It was shown that the net normal and tangential electrical stresses may tend to deform the drop in the same direction or in the opposite directions according to the deformation map that was introduced, comprised of the line of $\Phi_t = 0$ and curves of $\Phi_n = 0$ and $\Phi_n = 0$ drawn in $S - R$ coordinates.

APPENDIX A : THE ORDER OF ACCURACY OF THE SOLUTION

In seeking analytical solution to multifluid flow problems, one is generally faced with the difficulty of satisfying interfacial boundary conditions at an interface that does not coincide with the coordinate surfaces. For small interface deformation, this problem can be addressed by *the domain perturbation theory*, a regular perturbation expansion method that its formalism was introduced by Joseph [27]; however, it was around long before that (see the comments in page 283 of Ref. [28]). The essence of the method is to define a small perturbation parameter ε and to seek a solution of the form

$$\Lambda(\mathbf{r}) = \Lambda^0(\mathbf{r}) + \varepsilon\Lambda^1(\mathbf{r}) + O(\varepsilon^2) \tag{A1}$$

for the dependent variables Λ (velocity, electric potential, etc.) and to replace the exact boundary condition at the interface with an approximate boundary condition at a coordinate surface that is asymptotically equivalent for $\varepsilon \ll 1$ using the Taylor series expansion. Here Λ^0 and Λ^1 are called the solutions at the zeroth and the first order of the perturbation

parameter ε, respectively, and $\mathbf{r}$ represents the position vector of a point. In the language of domain perturbation theory, our solution for the field variables is of the zeroth order, while that for the deformation is of the first order.

To put our solution in perspective, in the following we outline the major steps that are involved in finding a first-order solution for the electric field potential ϕ. Here we need to solve Eq. (4) in the domains depicted in Fig. 1 and subject to the following jump conditions:

$$\phi_i(r,\theta)|_{r=\xi} = \phi_o(r,\theta)|_{r=\xi} \tag{A2}$$

and

$$\sigma_i \frac{\partial \phi_i}{\partial n}(r,\theta)\Big|_{r=\xi} = \sigma_o \frac{\partial \phi_o}{\partial n}(r,\theta)\Big|_{r=\xi} \tag{A3}$$

at a phase boundary that is represented by Eq. (8). Note that the subscripts i and o denote inside and outside, respectively, and that $\partial/\partial n$ denotes derivative in the direction normal to the interface. To proceed, we pick the deformation parameter as our perturbation parameter (i.e., $\varepsilon \equiv \mathcal{D}$) and rewrite Eq. (8) in the following form:

$$\xi = a + \varepsilon f(\theta), \tag{A4}$$

where $f(\theta) = (2/3)a(3\cos^2\theta - 1)$. We now seek a solution of the form

$$\phi = \phi^0(r,\theta) + \varepsilon\phi^1(r,\theta) + O(\varepsilon^2) \tag{A5}$$

for ϕ. Substitution of Eq. (A5) in Eq. (4) and grouping the terms that have the same coefficient in terms of the exponents of ε yield the electric field equations at the zeroth order

$$\nabla^2\phi^0 = 0 \tag{A6}$$

and at the first order

$$\nabla^2\phi^1 = 0. \tag{A7}$$

To find an appropriate form of boundary condition (A2) that is applicable at the coordinate surface, we use the Taylor series expansion of ϕ in the neighborhood of $r = a$:

$$\phi|_{r=\xi} = \phi\Big|_{r=a} + \varepsilon f(\theta)\frac{\partial\phi}{\partial r}\Big|_{r=a} \tag{A8}$$

and substitute for ϕ from Eq. (A5) in Eq. (A8). This yields

$$\phi|_{r=\xi} = \phi^0|_{r=a} + \varepsilon\left(\phi^1\Big|_{r=a} + f(\theta)\frac{\partial\phi^0}{\partial r}|_{r=a}\right) + O(\varepsilon^2). \tag{A9}$$

Substitution for $\phi_i|_{r=\xi}$ and $\phi_o|_{r=\xi}$ in boundary condition (A2) in terms of the expression in the right-hand side of Eq. (A9) and equating the terms that are of equal order of the exponents of ε in the left-hand side and the right-hand side of the resulting expression lead to the following expressions for boundary condition (A2) at the zeroth order

$$\phi_i^0(a,\theta) = \phi_o^0(a,\theta) \tag{A10}$$

and at the first order

$$\phi_i^1\Big|_{r=a} + f(\theta)\frac{\partial\phi_i^0}{\partial r}\Big|_{r=a} = \phi_o^1\Big|_{r=a} + f(\theta)\frac{\partial\phi_o^0}{\partial r}\Big|_{r=a}. \tag{A11}$$

To find the appropriate form of boundary condition (A3), we need to express the normal derivative in terms of the coordinate derivatives. Considering that $\partial\phi/\partial n = \nabla\phi\cdot\mathbf{n}$, $\nabla\phi = (\partial\phi/\partial r)\mathbf{e}_r + (1/r)(\partial\phi/\partial\theta)\mathbf{e}_\theta$, and $\mathbf{n} = \mathbf{e}_r - (\varepsilon/r)f'\mathbf{e}_\theta$ it is seen that

$$\frac{\partial\phi}{\partial n} = \frac{\partial\phi}{\partial r} - \varepsilon\frac{f'}{r}\frac{\partial\phi}{\partial\theta}, \tag{A12}$$

where $f' = df/d\theta$. We then expand the terms on the right-hand side of Eq. (A12) in the neighborhood of a using the Taylor series and substitute for ϕ from Eq. (A5) in the resulting expression. This leads to

$$\frac{\partial\phi}{\partial n}\Big|_{r=\xi} = \left[\frac{\partial\phi^0}{\partial r} + \varepsilon\left(f\frac{\partial^2\phi^0}{\partial r^2} + \frac{\partial\phi^1}{\partial r} - \frac{f'}{a}\frac{\partial\phi^0}{\partial\theta}\right)\right]\Big|_{r=a}. \tag{A13}$$

Substitution for $\partial\phi_i/\partial n|_{r=\xi}$ and $\partial\phi_o/\partial n|_{r=\xi}$ in Eq. (A3) in terms of the expression in the right-hand side of Eq. (A13) and equating the terms of the same order of exponents of ε results in the following expressions for the boundary condition (A3) at the zeroth order

$$\sigma_i\frac{\partial\phi_i^0}{\partial r}\Big|_{r=a} = \sigma_o\frac{\partial\phi_o^0}{\partial r}\Big|_{r=a} \tag{A14}$$

and at the first order

$$\sigma_i\left(f\frac{\partial^2\phi_i^0}{\partial r^2} - \frac{f'}{a}\frac{\partial\phi_i^0}{\partial\theta} + \frac{\partial\phi_i^1}{\partial r}\right)\Big|_{r=a} = \sigma_o\left(f\frac{\partial^2\phi_o^0}{\partial r^2} - \frac{f'}{a}\frac{\partial\phi_o^0}{\partial\theta} + \frac{\partial\phi_o^1}{\partial r}\right)\Big|_{r=a}. \tag{A15}$$

In summary we have two sets of equations and boundary conditions that need to be solved sequentially; namely, Eq. (A6) with boundary conditions (A10) and (A14), and Eq. (A7) with boundary conditions (A11) and (A15). In this study, we are only concerned with the results of a zeroth order solution for ϕ (see Ref. [1] and appendix of Ref. [18]), so we solved only for ϕ^0.

APPENDIX B : CALCULATION OF THE CURVATURE

The local curvature κ that is needed in the normal stress balance is the sum of the principal curvatures κ_1 and κ_2. While κ_1 and κ_2 can be found separately, an easier approach would be to calculate κ directly using

$$\kappa = \nabla\cdot\mathbf{n}, \tag{B1}$$

where $\mathbf{n}$ is the (outward) unit normal at the drop surface. For a general surface of the form $F(r,\theta,\varphi) = 0$, $\mathbf{n}$ can be found using

$$\mathbf{n} = \frac{\nabla F}{|\nabla F|}, \tag{B2}$$

where ∇ is the gradient operator in the spherical coordinates. Obviously, here the derivatives of F with respect to φ are all nil. We can further simplify the matter by taking advantage of the fact that the degree of deformation $\mathcal{D}$ is very small. Equation (8), therefore, can be written as $r = a + f(\theta)$, where $r \equiv \xi(t)$ and $f(\theta) = (2/3)a\mathcal{D}(3\cos^2\theta - 1) \ll a$. Carrying

out the calculation and ignoring the terms of order $\mathcal{D}^2$ and higher results in

$$\kappa = \frac{2}{r} - \frac{1}{r^2 \sin\theta}\frac{d}{d\theta}\left(\sin\theta \frac{df}{d\theta}\right). \tag{B3}$$

Substitution for r and $f(\theta)$ in Eq. (B3) and using the Taylor series expansion in terms of $\mathcal{D}$ results in

$$\kappa = \frac{2}{a} + \frac{8\mathcal{D}(3\cos^2\theta - 1)}{3a}. \tag{B4}$$

[1] G. I. Taylor, Proc. R. Soc. A **291**, 159 (1966).
[2] J. R. Melcher and G. I. Taylor, Annu. Rev. Fluid Mech. **1**, 111 (1969).
[3] C. V. Smith and J. R. Melcher, Phys. Fluids **10**, 2315 (1967).
[4] J. R. Melcher and W. Schwarz, Phys. Fluids **12**, 2604 (1968).
[5] J. R. Melcher and C. V. Smith, Phys. Fluids **12**, 778 (1969).
[6] O. Vizika and D. A. Saville, J. Fluid Mech. **239**, 1 (1992).
[7] J. Q. Feng and T. C. Scott, J. Fluid Mech. **311**, 289 (1996).
[8] E. Lac and G. M. Homsy, J. Fluid Mech. **590**, 239 (2007).
[9] H. A. Stone, A. D. Stroock, and A. Ajdari, Annu. Rev. Fluid Mech. **36**, 381 (2004).
[10] C. Sozou, Proc. R. Soc. London **334**, 343 (1973).
[11] R. J. Haywood, M. Renksizbulut, and G. D. Raithby, AIChE J. **37**, 1305 (1991).
[12] S. Moriya, K. Adachi, and T. Kotaka, Langmuir **2**, 155 (1985).
[13] T. Nishiwaki, K. Adachi, and T. Kotaka, Langmuir **4**, 170 (1988).
[14] C. T. O'Konski and H. C. Thacher, J. Phys. Chem. **57**, 955 (1953).
[15] G. Supeene, C. R. Koch, and S. Bhattacharjee, J. Comput. Theor. Nanosci. **1**, 429 (2004).
[16] D. L. Whitaker, C. Kim, C. L. Vicente, M. A. Weilert, H. J. Maris, and G. M. Seidel, Temp. Phys. **113**, 491 (1998).
[17] G. Supeene, C. R. Koch, and S. Bhattacharjee, J. Colloid Interface Sci. **318**, 463 (2008).
[18] M. N. Reddy and A. Esmaeeli, Int. J. Multiphase Flow **35**, 1051 (2009).
[19] R. S. Allan and S. G. Mason, Proc. R. Soc. London A **267**, 45 (1962).
[20] D. A. Saville, Annu. Rev. Fluid Mech. **29**, 27 (1997).
[21] C. Sozou, Proc. R. Soc. London **331**, 263 (1972).
[22] S. Torza, R. G. Cox, and S. G. Mason, Philos. Trans. R. Soc. London A **269**, 295 (1971).
[23] J. R. Lister and H. A. Stone, J. Fluid Mech. **317**, 275 (1996).
[24] J. M. Rallison, Annu. Rev. Fluid Mech. **16**, 45 (1984).
[25] J. C. Baygents, N. J. Rivette, and H. A. Stone, J. Fluid Mech. **368**, 359 (1998).
[26] M. N. Reddy, M.Sc. thesis. Southern Illinois University, 2008.
[27] D. D. Joseph, Arch. Ration. Mech. Anal. **24**, 325 (1967).
[28] L. G. Leal, *Advanced Transport Phenomena* (Cambridge University Press, New York, USA, 2007).